String Theory, Quantum Phase Transitions, and the Emergent Fermi Liquid

Mihailo Cubrovic *et al.*

Science **325**, 439 (2009);
DOI: 10.1126/science.1174962

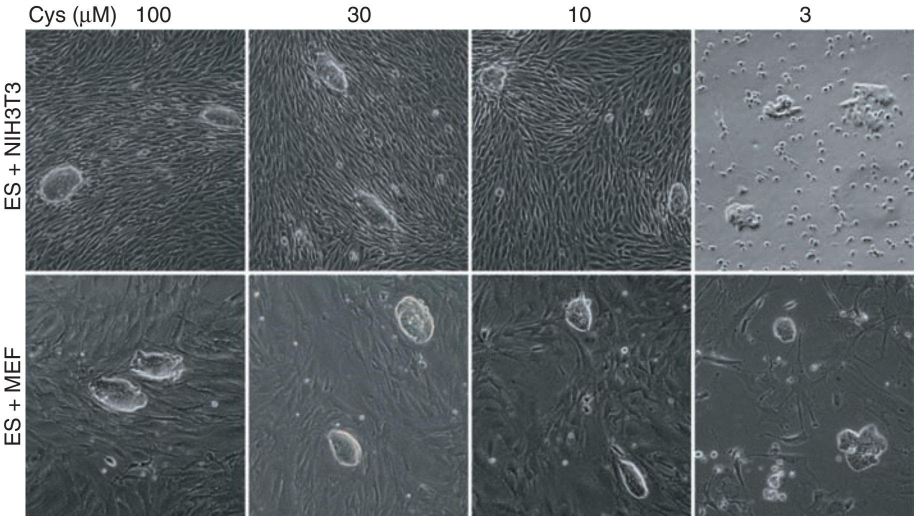

Fig. 6. Effects of cysteine deprivation on the growth of ES, MEF, and 3T3 cells. Cocultures of ES/MEF or ES/3T3 cells were subjected for 2 days to media containing varying amounts of supplemented cysteine. Cysteine deprivation severely impeded MEF cell growth at 10 and 3 μM and 3T3 growth at 3 μM (see also fig. S5). Although colony morphology was altered under the most severe conditions of cysteine deprivation, ES cell colonies were observed under all culture conditions tested.

of three inactivating mutations (*13*). Although highly conserved in gene organization, as well as primary amino acid sequence of the predicted TDH open reading frame, the human TDH gene carries AG-to-GG splice acceptor mutations in exons 4 and 6, as well as a nonsense mutation within exon 6 wherein arginine codon 214 is replaced by a translational stop codon. Whereas polymorphic variation within the human population has been observed for the exon 4 splice acceptor mutation, with some individuals carrying the normal AG splice acceptor dinucleotide and others carrying the GG variant, all individuals genotyped to date carry both the splice acceptor and nonsense mutations in exon 6. Reverse transcriptase–PCR analysis of TDH transcripts expressed in human fetal liver tissue showed complete skipping of exon 4 and either complete skipping or aberrant splicing of exon 6 (fig. S8). Given that exons 4 and 6 encode segments of the enzyme critical to its function and that truncation via the nonsense codon at amino acid 214 would also be predicted to yield an inactive variant, it appears that the human gene is incapable of producing an active TDH enzyme. Remarkably, all metazoans whose genomes have been sequenced to date, including chimpanzees, appear to contain an intact TDH gene (*14*). Unless humans evolved adaptive capabilities sufficient to overcome three mutational lesions, it would appear they are TDH deficient.

Human ES cells grow at a far slower rate than mouse ES cells, with a doubling time of 35 hours (*15*). Whether the slower growth rate of human ES cells reflects the absence of a functional TDH enzyme can perhaps be tested by introducing, into human ES cells, either a repaired human TDH gene or the intact TDH gene of a closely related mammal. That this strategy might work is supported by the expression in human cells of a functional form of the 2-amino-3-ketobutyrate-CoA ligase enzyme that converts the short-lived product of TDH-mediated catabolism of threonine into acetyl-CoA and glycine (Fig. 1B). It is possible that the culture conditions used to grow human ES cells do not match the ICM environment of the human embryo, in which the cell division cycle is more rapid than the 35-hour doubling time of cultured human ES cells (*16*). If human ES cells do not use the TDH enzyme to acquire an advantageous metabolic state for rapid growth, and if conditions can be adapted to facilitate the rapid proliferation of human ES cells in culture, the tools and approaches that we describe here may prove useful. As often happens in science, findings made in one experimental system can open avenues of investigation useful for other matters of inquiry. Finally, it is important to consider whether humans benefit from some form of selective advantage as a consequence of mutational inactivation of the TDH gene.

References and Notes

1. B. Alberts *et al*., in *Molecular Biology of the Cell* (Garland, New York, ed. 5, 2007), p. 1.
2. M. H. L. Snow, *J. Embryol. Exp. Morphol.* **42**, 293 (1977).
3. A. G. Smith, *Annu. Rev. Cell Dev. Biol.* **17**, 435 (2001).
4. B. P. Tu *et al*., *Proc. Natl. Acad. Sci. U.S.A.* **104**, 16886 (2007).
5. L. Warren, J. M. Buchanan, *J. Biol. Chem.* **229**, 613 (1957).
6. H. Weissbach, A. Peterkofsky, B. G. Redfield, H. Dickerman, *J. Biol. Chem.* **238**, 3318 (1963).
7. E. A. Phear, D. M. Greenberg, *J. Am. Chem. Soc.* **79**, 3737 (1957).
8. R. A. Dale, *Biochim. Biophys. Acta* **544**, 496 (1978).
9. E. Almaas, B. Kovacs, T. Vicsek, Z. N. Oltvai, A. L. Barabasi, *Nature* **427**, 839 (2004).
10. J. L. Hartman, *Proc. Natl. Acad. Sci. U.S.A.* **104**, 11,700 (2007).
11. T. Kazuoka *et al*., *J. Bacteriol.* **185**, 4483 (2003).
12. F. A. Brook, R. L. Gardner, *Proc. Natl. Acad. Sci. U.S.A.* **94**, 5709 (1997).
13. A. J. Edgar, *BMC Genet.* **3**, 18 (2002).
14. K. D. Pruitt, T. Tatusova, D. R. Maglott, *Nucleic Acids Res.* **35**, D61 (2007).
15. M. Amit *et al*., *Dev. Biol.* **227**, 271 (2000).
16. K. Hardy, A. H. Handyside, R. M. T. Winston, *Development* **107**, 597 (1989).
17. We thank B. Tu for the help with LC-MS/MS analysis; J. De Brabander and J. Ready for guidance on the chemical properties of threonine analogs; E. Olson for providing the AOK-5P line of iPS cells; D. Chong for technical assistance with in situ hybridization assays; and J. Goldstein, M. Rosen, and W. Neaves for helpful scientific input. This work was funded by an NIH Directors Pioneer Award, and unrestricted funds provided to S.L.M. by an anonymous donor.

Supporting Online Material

www.sciencemag.org/cgi/content/full/1173288/DC1
Materials and Methods
Figs. S1 to S8

9 March 2009; accepted 17 June 2009
Published online 9 July 2009;
10.1126/science.1173288
Include this information when citing this paper.

String Theory, Quantum Phase Transitions, and the Emergent Fermi Liquid

Mihailo Čubrović, Jan Zaanen, Koenraad Schalm*

A central problem in quantum condensed matter physics is the critical theory governing the zero-temperature quantum phase transition between strongly renormalized Fermi liquids as found in heavy fermion intermetallics and possibly in high–critical temperature superconductors. We found that the mathematics of string theory is capable of describing such fermionic quantum critical states. Using the anti–de Sitter/conformal field theory correspondence to relate fermionic quantum critical fields to a gravitational problem, we computed the spectral functions of fermions in the field theory. By increasing the fermion density away from the relativistic quantum critical point, a state emerges with all the features of the Fermi liquid.

Quantum many-particle physics lacks a general mathematical theory to deal with fermions at finite density. This is known as the "fermion sign problem": There is no recourse to brute-force lattice models because the statistical path-integral methods that work for any bosonic quantum field theory do not work for finite-density Fermi systems.

The nonprobabilistic fermion problem is known to be of exponential complexity (*1*), and in the absence of a general mathematical framework, all that remains is phenomenological guesswork in the form of the Fermi-liquid theory describing the state of electrons in normal metals and the mean-field theories describing superconductivity and other manifestations of spontaneous symmetry breaking. This problem has become particularly manifest in quantum condensed matter physics with the discovery of electron systems undergoing quantum phase transitions that are reminiscent of the bosonic quantum critical systems (*2*) but are governed by fermion statistics. Empirically well-documented examples are found in the "heavy fermion" intermetallics, where the zero-temperature transition occurs between different Fermi liquids with quasi-particle masses that diverge at the quantum critical point [(*3*) and references therein]. Such fermionic quantum critical states are believed to have a direct bearing on the problem of high–critical temperature (high-T_c) superconductivity because of the observation of quantum critical features in the normal state of optimally doped cuprate high-T_c superconductors [(*4*); (*5*) and references therein].

A large part of the fermion sign problem is to understand this strongly coupled fermionic quantum critical state. The emergent scale invariance and conformal symmetry at critical points is a benefit in isolating deep questions of principle. The fundamental problem is: How does the system get rid of the scales of Fermi energy and Fermi momentum that are intrinsically rooted in the workings of Fermi-Dirac statistics (*6*, *7*)? From another perspective, how can one construct a renormalization group with a relevant "operator" that describes the emergence of a statistics-controlled (heavy) Fermi liquid from the critical state (*3*), or perhaps the emergence of a high-T_c superconductor? Here, we show that a mathematical method developed in string theory has the capacity to answer at least some of these questions.

String theory for condensed matter. Our analysis makes use of the AdS/CFT correspondence: a duality relation between classical gravitational physics in a $d + 1$–dimensional "bulk" space-time with an anti–de Sitter (AdS) geometry and a strongly coupled conformal (quantum critical) field theory (CFT), with a large number of degrees of freedom, that occupies a flat or spherical d-dimensional "boundary" space-time. Applications of AdS/CFT to quantum critical systems have already been studied in the context of the quark-gluon plasma (*8*, *9*), superconductor-insulator transitions (*10*–*14*), and cold atom systems at the Feshbach resonance (*15*–*17*), but so far the focus has been on bosonic currents [see (*18*, *19*) and references therein]. Although AdS/CFT is convenient, in principle the ground state or any response of a bosonic statistical field theory can also be computed directly by averaging on a lattice. For fermions, statistical averaging is not possible because of the sign problem. There are, however, indications that AdS/CFT should be able to capture finite-density Fermi systems as well. Ensembles described through AdS/CFT can exhibit a specific heat that scales linearly with the temperature characteristic of Fermi systems (*20*), zero sound (*20*–*22*), and a minimum energy for fermionic excitations (*23*, *24*).

To address the question of whether AdS/CFT can describe finite-density Fermi systems and the Fermi liquid in particular, we compute the single charged fermion propagators and the associated spectral functions that are measured experimentally by angle-resolved photoemission spectroscopy ("AdS-to-ARPES") and indirectly by scanning tunneling microscopy. The spectral functions contain the crucial information regarding the nature of the fermion states. These are computed on the AdS side by solving for the on-shell (classical) Dirac equation in the curved AdS space-time background with sources at the boundary. A temperature T and finite $U(1)$ chemical potential μ_0 for electric charge is imposed in the field theory by studying the Dirac equation in the background of an AdS Reissner-Nordstrom black hole. We do so with the expectation that the $U(1)$ chemical potential induces a finite density of the charged fermions. The procedure to compute the retarded CFT propagator from the dual AdS description is then well established (*8*, *19*). Relative to the algorithm for computing bosonic responses, the treatment of Dirac waves in AdS is more delicate but straightforward; details are provided in (*25*). The equations obtained this way are solved numerically and the output is the retarded single fermion propagator $G_R(\omega, k)$ at finite T. Its imaginary part is the single fermion spectral function $A(\omega, k) = -(1/\pi)\,\mathrm{Im}\,\mathrm{Tr}[i\gamma^0 G_R(\omega, k)]$ that can be directly compared with ARPES experiments (*26*).

The reference point for this comparison is the quantum critical point described by a zero chemical potential ($\mu_0 = 0$), zero temperature ($T = 0$), and conformal and Lorentz invariant field theory. (Below, we use relativistic notation where $c = 1$.) Here the fermion propagators $\langle\bar{\Psi}\Psi\rangle \equiv G(\omega, k)$ are completely fixed by symmetry to be of the form

$$G^{\mathrm{CFT}}_{\Delta_\Psi}(\omega, k) \sim \frac{1}{\left(\sqrt{-\omega^2 + k^2}\right)^{d-2\Delta_\Psi}} \qquad (1)$$

where Δ_Ψ is the scaling dimension of the fermion field. Through the $\mathrm{AdS}_{d+1}/\mathrm{CFT}_d$ dictionary, Δ_Ψ is related to the mass parameter in the $d + 1$–dimensional AdS Dirac equation. Unitarity bounds this mass from below in units of the AdS radius $mL = \Delta_\Psi - d/2 > -\tfrac{1}{2}$ (we set $L = 1$ in the remainder). The choice of which value to use for m will prove essential to show the emergence of the Fermi liquid. The lower end of the unitarity-bound $m = -\tfrac{1}{2} + \delta$, $\delta << 1$, corresponds to introducing a fermionic conformal operator with weight $\Delta_\Psi = [(d-1)/2] + \delta$. This equals the scaling dimension of a nearly free fermion. Even though the underlying CFT is strongly coupled, the absence of a large anomalous dimension for a fermion with mass $m = -\tfrac{1}{2} + \delta$ argues that such an operator fulfills a spectator role and is only weakly coupled to this CFT. We therefore use such values in our calculations. Our expectation is that the Fermi liquid, as a system with well-defined quasi-particle excitations, can be described in terms of weakly interacting long-range fields. As we increase m from $m = -\tfrac{1}{2} + \delta$, the interactions increase and we can expect the quasi-particle description to cease to be valid beyond $m = 0$. For that value $m = 0$, and beyond $m > 0$, the naïve scaling dimension Δ_O of the fermion-bilinear $O_{\Delta_O} = \bar{\Psi}\Psi$ is marginal or irrelevant, and it is hard to see how the ultraviolet conformal theory can flow to a Fermi-liquid state, assuming that all vacuum state changes are caused by the condensation of bosonic oper-

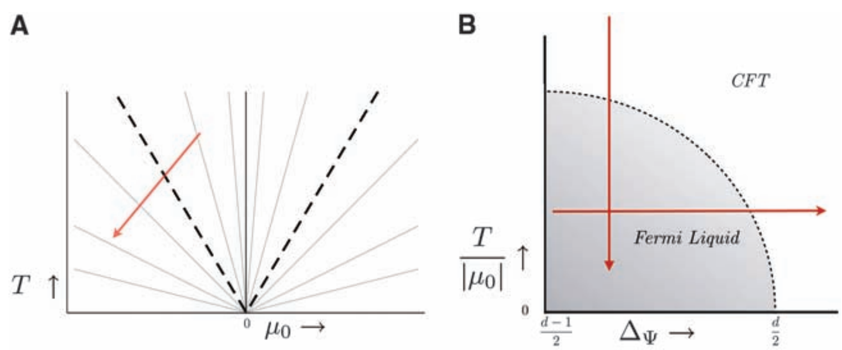

Fig. 1. (**A**) The phase diagram near a quantum critical point. Gray lines depict lines of constant μ_0/T; the spectral function of fermions is unchanged along each line if the momenta are appropriately rescaled. As we increase μ_0/T we cross over from the quantum critical regime to the Fermi liquid. (**B**) The trajectories in parameter space (μ_0/T, Δ_Ψ) studied here. We show the crossover from the quantum critical regime to the Fermi liquid by varying μ_0/T while keeping Δ_Ψ fixed; we cross back to the critical regime varying $\Delta_\Psi \to d/2$ for μ_0/T fixed. The boundary region is not an exact curve but only a qualitative indication.

Institute-Lorentz for Theoretical Physics, Leiden University, P.O. Box 9506, Leiden, Netherlands.

*To whom correspondence should be addressed. E-mail: kschalm@lorentz.leidenuniv.nl

ators. This intuition is borne out by our results: When $m \geq 0$, the standard Fermi liquid disappears. A similar approach to describing fermionic quantum criticality (*27*) discusses the special case $m = 0$ or $\Delta_\Psi = d/2$ in detail; an early attempt to describe the $m = 0$ system is (*28*).

The emergent Fermi liquid. With an eye toward experiment, we consider the AdS_4 dual to a relativistic CFT_3 in $d = 2 + 1$ dimensions (*25*). We do not know the detailed microscopic CFT, nor do we know whether a dual AdS with fermions as the sole $U(1)$ charged field exists as a fully quantum-consistent theory for all values of $m = \Delta_\Psi - d/2$, but the behavior of fermion spectral functions at a strongly coupled quantum critical point can be deduced nonetheless. Aside from Δ_Ψ, the spectral function will depend on the dimensionless ratio μ_0/T as well as the $U(1)$ charge g of the fermion; we set $g = 1$ from here on, as we expect that only large changes away from $g = 1$ will change our results qualitatively. We therefore study the system as a function of μ_0/T and Δ_Ψ. Our approach is sketched in Fig. 1B. We first study the spectral behavior as a function of μ_0/T for fixed $\Delta_\Psi < 3/2$; then we study the spectral behavior as we vary the scaling dimension Δ_Ψ from 1 to $3/2$ for fixed μ_0/T coding for an increasingly interacting fermion. Note that our setup and numerical calculations necessitate a finite value of μ_0/T; all our results are at nonzero T.

Our analysis starts near the reference point $\mu_0/T \to 0$, where the long-range behavior of the system is controlled by the quantum critical point (Fig. 1A). Here we expect to recover conformal invariance, as the system forgets about any well-defined scales, and the spectral function should be controlled by the branchcut at $\omega = k$ in the Green's function (Eq. 1): (i) For $\omega < k$ it should vanish. (ii) At $\omega = k$ we expect a sharp peak, which for $\omega >> k$ scales as $\omega^{2\Delta_\Psi - d}$. Figure 2A shows this expected behavior of spectral function for three different values of the momentum for a fermionic operator with weight $\Delta_\Psi = 5/4$ computed from AdS_4 following the setup in (*25*).

Turning on μ_0/T while holding $\Delta_\Psi = 5/4$ fixed shifts the center location of the two branchcuts to an effective chemical potential $\omega = \mu_{eff}$; this bears out our expectation that the $U(1)$ chemical potential induces a finite fermion density. Although the peak at the location of the negative branchcut $\omega \sim \mu_{eff} - k$ stays broad, the peak at the other branchcut $\omega \sim \mu_{eff} + k$ sharpens distinctly as the size of μ_0/T is increased (Fig. 2B). We identify this peak with the quasi-particle of the Fermi liquid and its appearance as the crossover between the quantum critical regime and the Fermi-liquid regime. The spectral properties of the Fermi liquid are very well known and display a number of uniquely identifying characteristics (*29*, *30*). If this identification is correct, all these characteristics must be present in our spectra as well.

1) The quasi-particle peak should approach a delta function at the Fermi momentum $k = k_F$. In Fig. 2B we see the peak narrow as we increase k, then peak and broaden back out as we pass $k \sim k_F$ (recall that $T = 0$ is outside our numerical control and the peak always has some broadening). In addition, the spectrum should vanish identically at the Fermi energy $A(\omega = E_F, k) = 0$, independent of k (Fig. 2C).

2) The quasi-particle should have linear dispersion relation near the Fermi energy with a renormalized Fermi velocity v_F different from the underlying relativistic speed $c = 1$. In Fig. 3 we plot the maximum of the peak ω_{max} as a function of k. At high k we recover the linear dispersion relation $\omega = |k|$ underlying the Lorentz invariant branchcut in Eq. 1. Near the Fermi energy and Fermi momentum, however, this dispersion relation changes to a slope $v_F \equiv \lim_{\omega \to E_F, k \to k_F} (\omega - E_F)/(k - k_F)$ clearly less than unity.

Note that the Fermi energy E_F is not located at zero frequency. Recall, however, that the AdS chemical potential μ_0 is the bare $U(1)$ chemical potential in the CFT. This is confirmed in Fig. 3 from the high-k behavior: Its Dirac point is μ_0. On the other hand, the chemical potential felt by the IR fermionic degrees of freedom is renormalized to the value $\mu_F = \mu_0 - E_F$. As is standard, the effective energy $\tilde{\omega} = \omega - E_F$ of the quasi-particle is measured with respect to E_F.

3) At low temperatures, Fermi-liquid theory predicts the width of the quasi-particle peak to

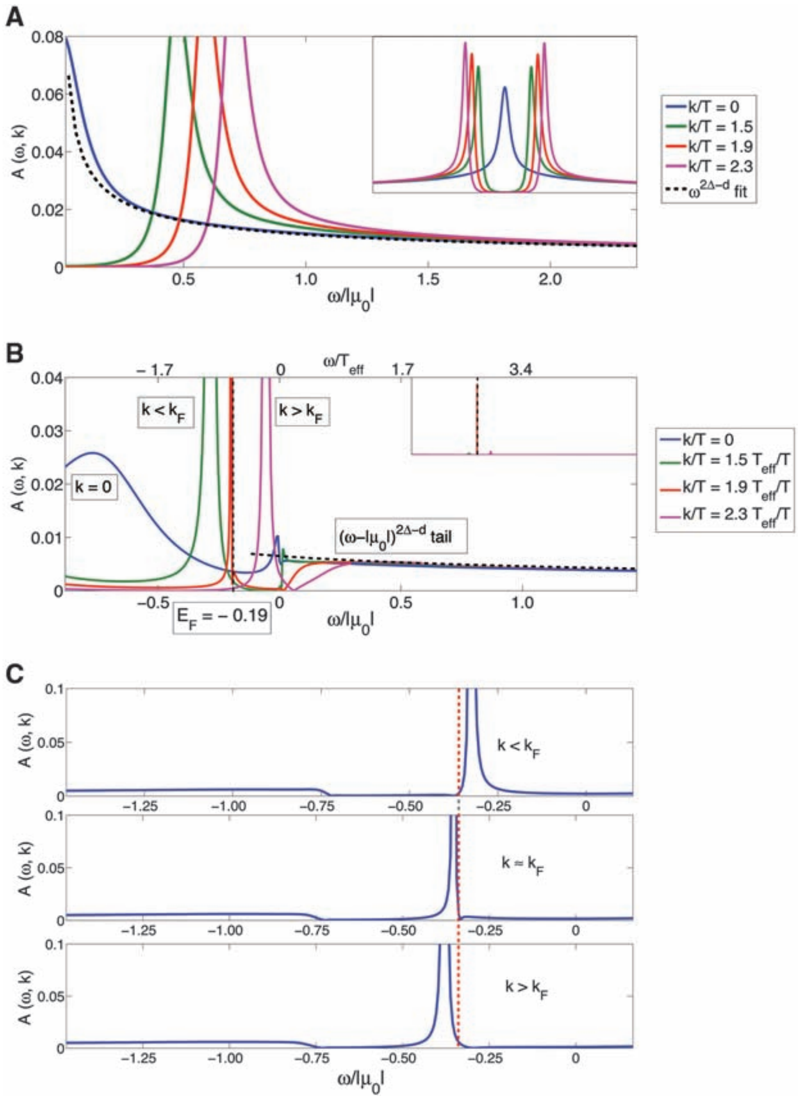

Fig. 2. (**A**) The spectral function $A(\omega,k)$ for $\mu_0/T = 0.01$ and $m = -1/4$. The spectral function has the asymptotic branchcut behavior of a conformal field of dimension $\Delta_\Psi = d/2 + m = 5/4$: It vanishes for $\omega < k$, save for a finite T tail, and for large ω it scales as $\omega^{2\Delta_\Psi - d}$. (**B**) The emergence of the quasi-particle peak as we change the chemical potential to $\mu_0/T = -30.9$ for the same value $\Delta_\Psi = 5/4$. The three displayed momenta k/T are rescaled by a factor T_{eff}/T for the most meaningful comparison with those in (A) (*25*). The insets show the full scales of the peak heights and the dominance of the quasi-particle peak for $k \sim k_F$. (**C**) Vanishing of the spectral function at E_F for $\Delta_\Psi = 1.05$ and $\mu_0/T = -30.9$. The deviation of the dip location from E_F is a finite temperature effect; it decreases with increasing μ_0/T.

grow quadratically with temperature. Figure 4, A and B, shows this distinctive behavior up to a critical temperature, $T_c/\mu_0 \sim 0.16$. This temperature behavior directly follows from the fact that the imaginary part of the self-energy $\Sigma(\omega, k) = \omega - k - [\mathrm{Tr}\; i\gamma^0 G(\omega, k)]^{-1}$ should have no linear term when expanded around E_F: Im $\Sigma(\omega, k) \sim (\omega - E_F)^2 + \ldots$ This is shown in Fig. 4, C and D.

These results give us confidence that we have identified the characteristic quasi-particles at the Fermi surface of the Fermi liquid emerging from the quantum critical point.

We now discuss how this Fermi liquid evolves when we increase the bare μ_0 (Fig. 5). Similar to the fermion chemical potential μ_F, the fundamental control parameter of the Fermi liquid, the fermion density ρ_F, is not directly related to the AdS μ_0. We can, however, infer it from the Fermi momentum k_F that is set by the quasi-particle pole via Luttinger's theorem $\rho_F \sim k_F^{d-1}$. The more illustrative figure is therefore Fig. 5B, which shows the quasi-particle characteristics as a function of k_F/T. We find that the quasi-particle velocities decrease slightly with increasing k_F, rapidly leveling off to a finite constant less than the relativistic speed. Thus, the quasi-particles become increasingly heavy as their mass $m_F \equiv k_F/v_F$ approaches linear growth with k_F. The Fermi energy E_F also shows linear growth. Suppose the heavy Fermi–quasi-particle system has the underlying canonical nonrelativistic dispersion relation $E = k^2/(2m_F) = k_F^2/(2m_F) + v_F(k - k_F) + \ldots$; in that case, the observed Fermi energy E_F should equal the renormalized Fermi energy $E_F^{(\mathrm{ren})} \equiv k_F^2/(2m_F)$. Figure 5B shows that these energies E_F and $E_F^{(\mathrm{ren})}$

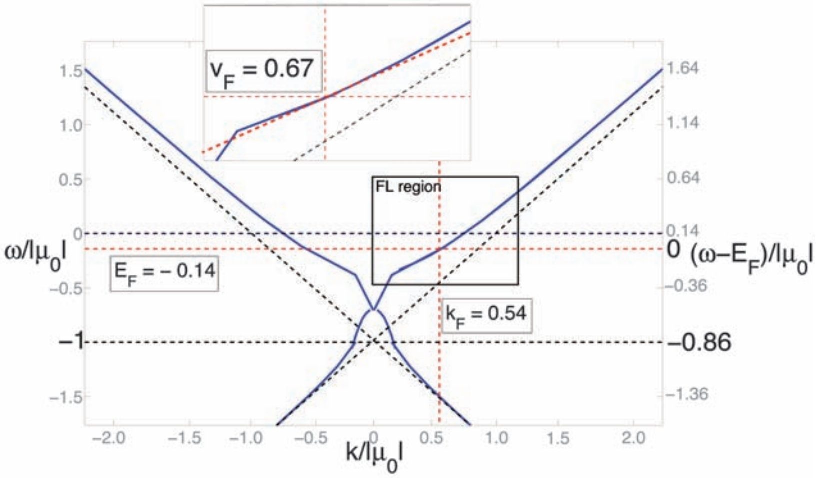

Fig. 3. Maxima in the spectral function as a function of k/μ_0 for $\Delta_\Psi = 1.35$ and $\mu_0/T = -30.9$. Asymptotically for large k the negative-k branchcut recovers the Lorentz-invariant linear dispersion with unit velocity, but with the zero shifted to $-\mu_0$. The peak location of the positive-k branchcut that changes into the quasi-particle peak changes noticeably. It gives the dispersion relation of the quasi-particle near (E_F, k_F). The change of the slope from unity shows renormalization of the Fermi velocity. This is highlighted in the inset. Note that the Fermi energy E_F is not located at $\omega_{AdS} = 0$. The AdS calculation visualizes the renormalization of the bare chemical potential $\mu_0 = \mu_{AdS}$ to the effective chemical potential $\mu_F = \mu_0 - E_F$ felt by the low-frequency fermions.

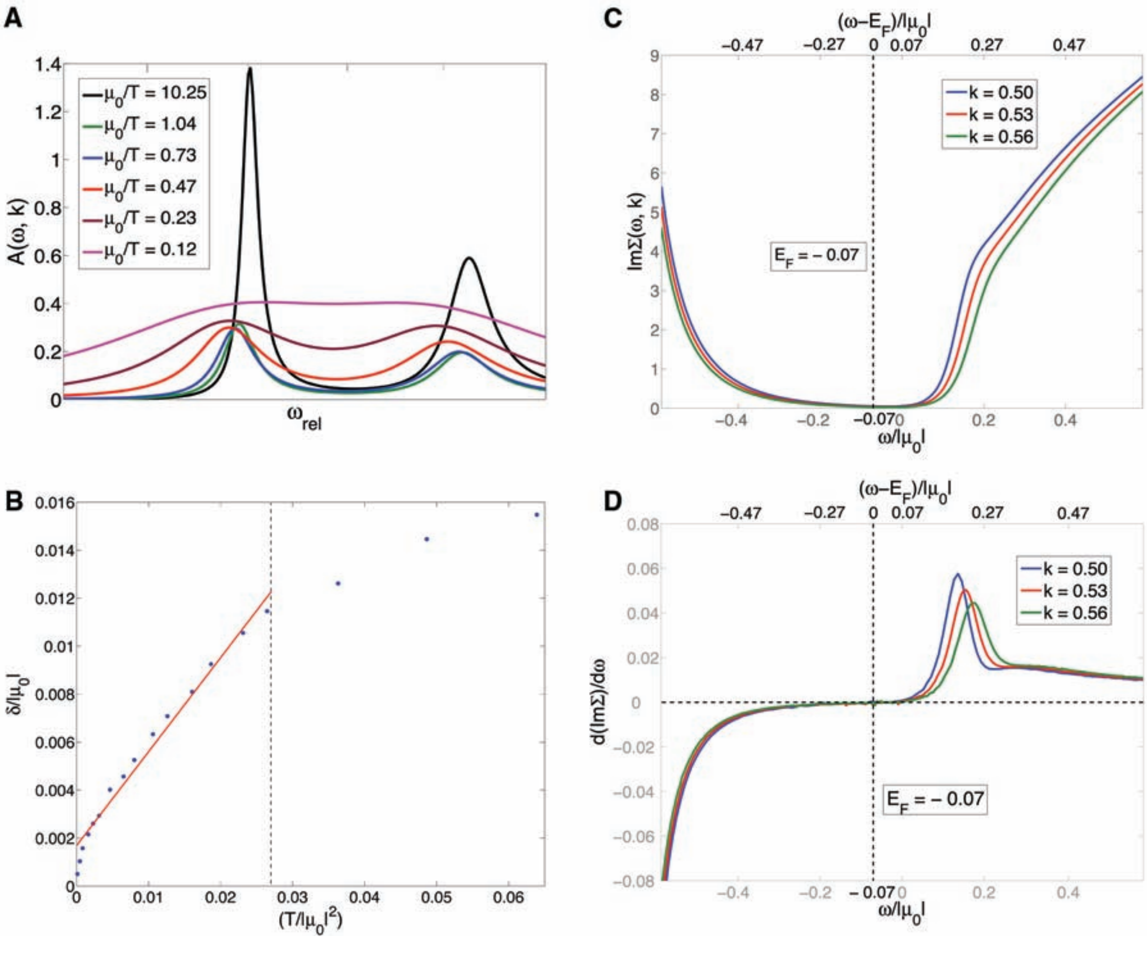

Fig. 4. (**A**) Temperature dependence of the quasi-particle peak for $\Delta_\Psi = 5/4$ and $k/k_F \approx 0.5$; all curves have been shifted to a common peak center. (**B**) The quasi-particle peak width $\delta \sim$ Re $\Sigma(\omega, k = k_F)$ for $\Delta_\Psi = 5/4$ as a function of T^2; it reflects the expected behavior $\delta \sim T^2$ up to a critical temperature T_c/μ_0, beyond which the notion of a quasi-particle becomes untenable. (**C** and **D**) The imaginary part of the self-energy $\Sigma(\omega, k)$ near E_F, k_F for $\Delta_\Psi = 1.4$, $\mu_0/T = -30.9$. The defining Im $\Sigma(\omega, k) \sim (\omega - E_F)^2 + \ldots$ dependence for Fermi-liquid quasi-particles is faint in (C) but obvious in (D). It shows that the intercept of ∂_ω Im $\Sigma(\omega, k)$ vanishes at E_F, k_F.

track each other remarkably well. We therefore infer that the true zero of energy of the Fermi quasi-particle is set by the renormalized Fermi energy as deduced from the Fermi velocity and Fermi momentum.

Although the true quasi-particle behavior disappears at $T > T_c$, Fig. 5A indicates that in the limit $k_F/T \rightarrow 0$ the quasi-particle pole strength vanishes, $Z_k \rightarrow 0$, while the Fermi velocity v_F remains finite; v_F approaches the bare velocity $v_F = 1$. This is seemingly at odds with the heavy Fermi liquid relation $Z_k \sim m_{micro}/m_F = m_{micro}v_F/k_F$. The resolution is the restoration of Lorentz invariance at zero density. From general Fermi liquid considerations it follows that $v_F = Z_k\,(1 + \partial_k \text{ Re } \Sigma|_{E_F, k_F})$ and $Z_k = 1/(1 - \partial_\omega \text{ Re } \Sigma|_{E_F, k_F})$, where $\partial_{k,\omega}$ Re Σ refers to the momentum and energy derivatives of the real part of the fermion self-energy $\Sigma(\omega, k)$ at k_F, E_F. Lorentz invariance imposes $\partial_\omega \Sigma' = -\,\partial_k \Sigma'$, which allows for vanishing Z_k with $v_F \rightarrow 1$. Interestingly, the case has been made that such a relativistic fermionic behavior might be underlying the physics of cuprate high-T_c superconductors (*31*).

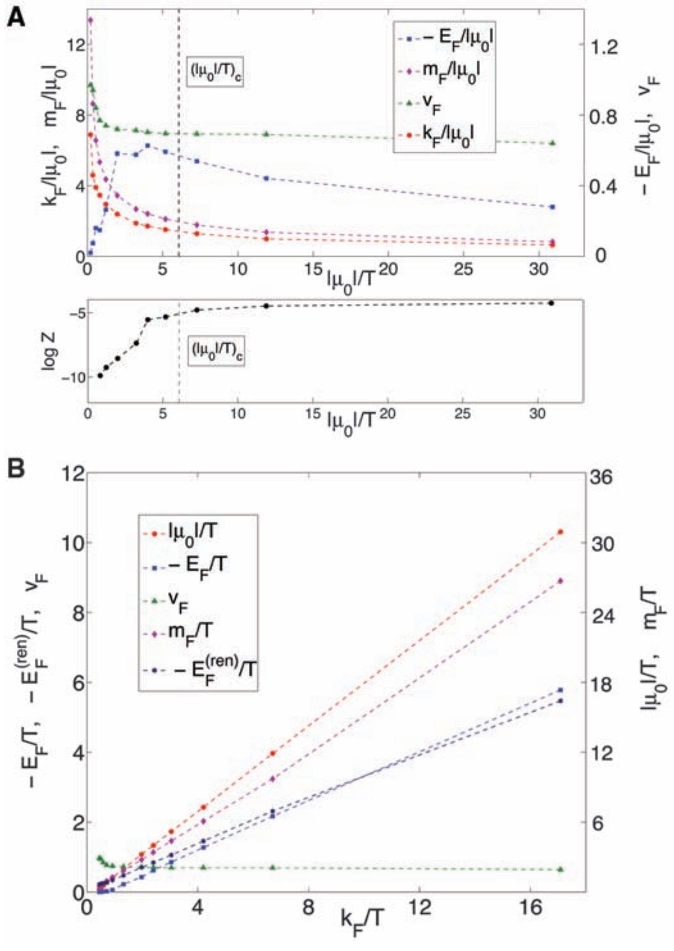

Fig. 5. The quasi-particle characteristics as a function of μ_0/T for $\Delta_\Psi = 5/4$. (**A**) The change of k_F, v_F, m_F, E_F, and the pole strength Z (the total weight between half-maxima) as we change μ_0/T. Beyond a critical value $(\mu_0/T)_c$ we lose the characteristic T^2 broadening of the peak and there is no longer a real quasi-particle, although the peak is still present. For the Fermi liquid, k_F/T rather than μ_0/T is the defining parameter. (**B**) We can invert this relation, and (B) shows the quasi-particle characteristics as a function of k_F/T. Note the linear relationships of m_F and E_F to k_F and that the renormalized Fermi energy $E^{(ren)} \equiv k_F^2/(2m_F)$ matches the empirical value E_F remarkably well.

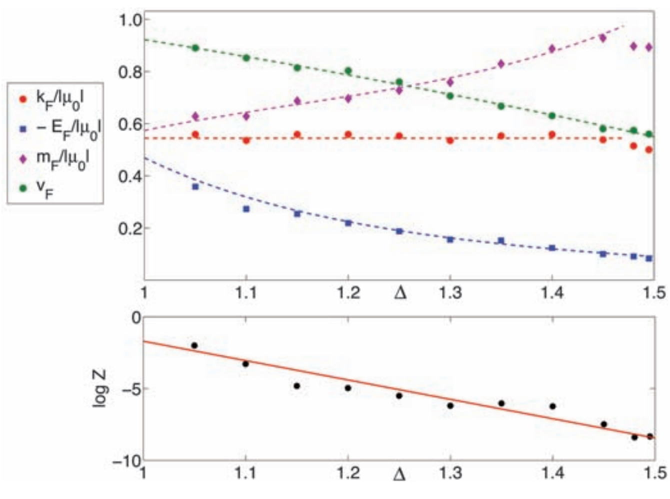

Fig. 6. The quasi-particle characteristics as a function of the Dirac fermion mass $-^1\!/_2 < m < 0$ corresponding to $1 < \Delta_\Psi < {}^3\!/_2$ for $\mu_0/T = -30.9$. The upper panel shows the independence of k_F of the mass. This indicates Luttinger's theorem if the anomalous dimension Δ_Ψ is taken as an indicator of the interaction strength. Note that v_F and E_F both approach finite values as $\Delta_\Psi \rightarrow {}^3\!/_2$. The lower panel shows the exponential vanishing pole strength Z (the integral between the half-maxima) as $m \rightarrow 0$.

Finally, we address the important question of what happens when we vary the conformal dimension Δ_Ψ of the fermionic operator. Figure 6 shows that the Fermi momentum k_F stays constant as we increase Δ_Ψ. This completes our identification of the new phase as the Fermi liquid: It indicates that the AdS dual obeys Luttinger's theorem, if we can interpret the conformal dimension of the fermionic operator as a proxy for the interaction strength. We find furthermore that the quasi-particle pole strength vanishes as we approach $\Delta_\Psi = {}^3\!/_2$. This confirms our earlier assumption that it is essential to study the system for $\Delta_\Psi < d/2$ and that the point $\Delta_\Psi = d/2$, where the naïve fermion bilinear becomes marginal, signals the onset of a new regime. Because the fermion bilinear is marginal at that point, this ought to be an interesting regime in its own right, and we refer to (*27*) for a discussion thereof (*32*). Highly remarkable is that the pole strength vanishes in an exponential fashion rather than the anticipated algebraic behavior (*6*, *7*). This could indicate that an essential singularity governs the critical point at $\Delta_\Psi = d/2$, and we note that such a type of behavior was identified by Lawler *et al.* in their analysis of the Pomeranchuk instability in $d = 2 + 1$ dimensions using the Haldane patching bosonization procedure (*33*). Note that this finite μ_0/T transition as we vary Δ_Ψ has no clear symmetry change, similar to (*7*). However, this may be an artifact of the fact that our theory is not quantum mechanically complete (*25*). Note also that the quasi-particle velocity and the renormalized Fermi energy $E_F = v_F(k - k_F) - E$ stay finite at the $\Delta_\Psi = {}^3\!/_2$ transition with $Z \rightarrow 0$, which could indicate an emergent Lorentz invariance for the reasons discussed above.

Concluding remarks. We have presented evidence that the AdS dual description of strongly coupled field theories can describe the emergence of the Fermi liquid from a quantum critical state, as a function of both density and interaction strength, as encoded in the conformal dimension of the fermionic operators. From the AdS gravity perspective, it was unclear whether this would happen. Sharp peaks in the CFT spectral function correspond to so-called quasi-normal modes of black holes (*34*), but Dirac quasi-normal modes have received little study [see, e.g., (*35*)]. It is remarkable that the AdS calculation processes the Fermi-Dirac statistics essential to the Fermi liquid correctly. This is manifested by the emergent renormalized Fermi energy and the validity of Luttinger's theorem. The AdS gravity computation, however, is completely classical without explicit quantum statistics, although we do probe the system with a fermion. It would therefore be interesting to fully understand the AdS description of what is happening, in particular how the emergent scales

E_F and k_F feature in the geometry. An early indication of such scales was seen in (*24*, *36*) in a variant of the story that geometry is not universal in string theory: The geometry depends on the probe used, and different probes experience different geometric backgrounds. The absence of these scales in the general relativistic description of the AdS black hole could thus be an artifact of the Riemannian metric description of space-time.

Regardless of these questions, AdS/CFT has shown itself to be a powerful tool to describe finite-density Fermi systems. The description of the emergent Fermi liquid presented here argues that AdS/CFT is uniquely suited as a computational device for field theory problems suffering from fermion sign problems. AdS/CFT represents a rich mathematical environment and a new approach to qualitatively and quantitatively investigate important questions in quantum many-body theory at finite fermion density.

References and Notes

1. M. Troyer, U. J. Wiese, *Phys. Rev. Lett.* **94**, 170201 (2005).
2. S. Sachdev, *Quantum Phase Transitions* (Cambridge Univ. Press, Cambridge, 1999).
3. J. Zaanen, *Science* **319**, 1295 (2008).
4. D. van der Marel *et al*., *Nature* **425**, 271 (2003).
5. J. Zaanen, *Nature* **430**, 512 (2004).
6. T. Senthil, *Phys. Rev. B* **78**, 035103 (2008).
7. F. Krüger, J. Zaanen, *Phys. Rev. B* **78**, 035104 (2008).
8. D. T. Son, A. O. Starinets, *Annu. Rev. Nucl. Part. Sci.* **57**, 95 (2007).
9. S. S. Gubser, A. Karch, http://arxiv.org/abs/0901.0935 (2009).
10. C. P. Herzog, P. Kovtun, S. Sachdev, D. T. Son, *Phys. Rev. D* **75**, 085020 (2007).
11. S. A. Hartnoll, P. K. Kovtun, M. Muller, S. Sachdev, *Phys. Rev. B* **76**, 144502 (2007).
12. S. S. Gubser, *Phys. Rev. D* **78**, 065034 (2008).
13. S. A. Hartnoll, C. P. Herzog, G. T. Horowitz, *Phys. Rev. Lett.* **101**, 031601 (2008).
14. S. A. Hartnoll, C. P. Herzog, G. T. Horowitz, *J. High Energy Phys.* **0812**, 015 (2008).
15. D. T. Son, *Phys. Rev. D* **78**, 046003 (2008).
16. K. Balasubramanian, J. McGreevy, *Phys. Rev. Lett.* **101**, 061601 (2008).
17. A. Adams, K. Balasubramanian, J. McGreevy, *J. High Energy Phys.* **0811**, 059 (2008).
18. S. A. Hartnoll, *Science* **322**, 1639 (2008).
19. S. A. Hartnoll, http://arxiv.org/abs/0903.3246 (2009).
20. M. Kulaxizi, A. Parnachev, *Nucl. Phys. B* **815**, 125 (2009).
21. A. Karch, D. T. Son, A. O. Starinets, *Phys. Rev. Lett.* **102**, 051602 (2009).
22. M. Kulaxizi, A. Parnachev, *Phys. Rev. D* **78**, 086004 (2008).
23. L. Brits, M. Rozali, http://arxiv.org/abs/0810.5321 (2008).
24. H. H. Shieh, G. van Anders, *J. High Energy Phys.* **0903**, 019 (2009).
25. See supporting material on *Science* Online.
26. ARPES Fermi-surface measurements assume that electrons are the only relevant charged objects. If this is so, then it measures the electron (i.e., fermion) spectral function. This spectral function is what we compute here, even though in our AdS setup the fermions are almost certainly not the only charged objects.
27. H. Liu, J. McGreevy, D. Vegh, http://arxiv.org/abs/0903.2477 (2009).
28. S. S. Lee, *Phys. Rev. D* **79**, 086006 (2009).
29. E. M. Lifshitz, L. P. Pitaevskii, *Statistical Physics, Part 2* (Pergamon, Oxford, 1980).
30. H. J. Schulz, G. Cuniberti, P. Pieri, in *Field Theories for Low-Dimensional Condensed Matter Systems*, G. Morandi, P. Sodano, A. Tagliacozzo, V. Tognetti, Eds. (Springer, Berlin, 2000), chap. 2.
31. M. Randeria, A. Paramekanti, N. Trivedi, *Phys. Rev. B* **69**, 144509 (2004).
32. Note that the $m = 0$ spectral peak discussed in (*27*) is therefore not the peak we identified with the quasi-particle state. See (*25*).
33. M. J. Lawler, V. Fernandez, D. G. Barci, E. Fradkin, L. Oxman, *Phys. Rev. B* **73**, 085101 (2006).
34. P. K. Kovtun, A. O. Starinets, *Phys. Rev. D* **72**, 086009 (2005).
35. H. T. Cho, A. S. Cornell, J. Doukas, W. Naylor, *Phys. Rev. D* **77**, 016004 (2008).
36. M. Rozali, H. H. Shieh, M. Van Raamsdonk, J. Wu, *J. High Energy Phys.* **0801**, 053 (2008).

37. We thank F. Denef, S. Hartnoll, H. Liu, J. McGreevy, S. Sachdev, D. Sadri, and D. Vegh for discussions. Supported by a VIDI Innovative Research Incentive Grant (K.S.) from the Netherlands Organization for Scientific Research (NWO) and by a Spinoza Award (J.Z.) from NWO and the Dutch Foundation for Fundamental Research on Matter (FOM).

Supporting Online Material

www.sciencemag.org/cgi/content/full/1174962/DC1
SOM Text
Fig. S1
References

14 April 2009; accepted 16 June 2009
Published online 25 June 2009;
10.1126/science.1174962
Include this information when citing this paper.

Radio Imaging of the Very-High-Energy γ-Ray Emission Region in the Central Engine of a Radio Galaxy

The VERITAS Collaboration, the VLBA 43 GHz M87 Monitoring Team, the H.E.S.S. Collaboration, the MAGIC Collaboration*

The accretion of matter onto a massive black hole is believed to feed the relativistic plasma jets found in many active galactic nuclei (AGN). Although some AGN accelerate particles to energies exceeding 10^{12} electron volts and are bright sources of very-high-energy (VHE) γ-ray emission, it is not yet known where the VHE emission originates. Here we report on radio and VHE observations of the radio galaxy Messier 87, revealing a period of extremely strong VHE γ-ray flares accompanied by a strong increase of the radio flux from its nucleus. These results imply that charged particles are accelerated to very high energies in the immediate vicinity of the black hole.

Active galactic nuclei (AGN) are extragalactic objects thought to be powered by massive black holes in their centers. They can show strong emission from the core, which is often dominated by broadband continuum radiation ranging from radio to x-rays and by substantial flux variability on different time scales. More than 20 AGN have been established as very-high-energy (VHE) γ-ray emitters with measured energies above 0.1 TeV; the jets of most of these sources are believed to be aligned with the line of sight to within a few degrees. The size of the VHE γ-ray emission region can generally be constrained by the time scale of the observed flux variability (*1*, *2*), but its location remains unknown.

We studied the inner structure of the jet of the giant radio galaxy Messier 87 (M87), a known VHE γ-ray–emitting AGN (*2*–*5*) with a (6.0 ± 0.5) × 10^9 solar mass black hole (*6*) (scaled by distance), located 16.7 Mpc (54 million light years) away in the Virgo cluster of galaxies. The angle between its plasma jet and the line of sight is estimated to lie between 15° and 25° [see supporting online material (SOM) text]. The substructures of the jet, which are expected to scale with the Schwarzschild radius R_s of the black hole (*7*), are resolved in the x-ray, optical, and radio wave bands (*8*) (Fig. 1). High-frequency radio very-long-baseline interferometry (VLBI) observations with resolution under a milli–arc second (milli–arc sec) are starting to probe the collimation region of the jet (*9*). With its proximity, bright and well-resolved jet, and very massive black hole, M87 provides a unique laboratory in which to study relativistic jet physics in connection with the mechanisms of VHE γ-ray emission in AGN.

VLBI observations of the M87 inner jet show a well-resolved, edge-brightened structure extending to within 0.5 milli–arc sec (0.04 pc or 70 R_s) of the core. Closer to the core, the jet has a wide opening angle, suggesting that this is the collimation region (*9*). Generally, the core can be offset from the actual location of the black hole by an unknown amount (*10*), in which case it could mark the location of a shock structure or the region where the jet becomes optically thin. However, in the case of M87, a weak structure

*The full list of authors and affiliations is presented at the end of this paper.